

PAPER • OPEN ACCESS

Positron scattering and transport in liquid helium

To cite this article: D G Cocks *et al* 2020 *J. Phys. B: At. Mol. Opt. Phys.* **53** 225201

View the [article online](#) for updates and enhancements.



IOP | ebooks™

Bringing together innovative digital publishing with leading authors from the global scientific community.

Start exploring the collection—download the first chapter of every title for free.

Positron scattering and transport in liquid helium

D G Cocks¹ , R P McEachran¹, G J Boyle² , E Cheng¹ and R D White^{3,*} 

¹ Research School of Physics, Australian National University, Canberra, Australia

² Linear Accelerator Technologies, Deutsches Elektronen-Synchrotron, Hamburg, Germany

³ College of Science, James Cook University, Townsville, Australia

E-mail: ronald.white@jcu.edu.au

Received 13 April 2020, revised 13 July 2020

Accepted for publication 18 August 2020

Published 9 October 2020



Abstract

In previous papers we have proposed a method for the *ab initio* calculation of fully differential cross-sections for electron scattering in liquids and applied it to liquid argon, xenon and krypton. In this paper, we extend the procedure to the consideration of positron scattering in liquid helium, which is complicated by the annihilation process as well as the fact that the electron definition for the region ‘owned’ by a target atom used previously does not have a positron analogue. We explore several physically motivated definitions to obtain effective positron scattering in the dense fluid. We find that our calculations of a pure helium system cannot precisely match experimental measurements, however by including a small admixture (<0.1%) of an impurity, we can obtain reasonable agreement in the dense gas phase. In contrast, the comparison between our calculations and liquid phase measurements is less satisfactory. This provides motivation to explore further multiple scattering effects in the theory.

Keywords: positrons, dense fluids, transport, non-equilibrium

(Some figures may appear in colour only in the online journal)

1. Introduction

Positrons are used in a variety of diagnostic applications, including the medical diagnostic of positron emission tomography, materials analysis through positron annihilation lifetime spectroscopy and Doppler broadening spectroscopy [1]. Positrons can even be used as an indirect probe of the structure of the Galaxy [2]. These experimental techniques generally rely on the interpretation of gamma rays emitted from the annihilation of the positrons with electrons.


To be able to interpret these diagnostics, it is essential to understand how the positron propagates through the material under investigation. As the concentration of positrons is typically very low, this falls under the umbrella of swarm modelling [3]. In gases this is usually explored through kinetic

theory simulations, which allows for a simple scaling with density for transport properties such as annihilation rates and drift velocities. As the density significantly increases, these scaling behaviours have historically been used directly, even for systems as dense as liquids where the scaling laws break down.

To model charged particle transport in liquids and dense gases, we must account for effects such as multiple scattering and interaction screening, using correlations between particles in the fluid. This was first described by Lekner [4] and we have since extended the procedure to calculate more accurate, *ab initio*, fully-differential effective elastic cross sections for electrons propagating in liquid argon, xenon and krypton [5–7] using only the pair correlator for each fluid.

In this article, we investigate positron transport. On the one hand, this should share much of the same properties of electron transport through a fluid, as both the electron and positron are a light charged particle. On the other hand, the interaction of the positron with a single atom of the fluid is very different: it has no exchange interaction, the sign of the Coulomb interaction is reversed and loss processes are always present, even

* Author to whom any correspondence should be addressed.

 Original content from this work may be used under the terms of the [Creative Commons Attribution 4.0 licence](https://creativecommons.org/licenses/by/4.0/). Any further distribution of this work must maintain attribution to the author(s) and the title of the work, journal citation and DOI.

as the collisional energy approaches zero. Note, however, that the polarisation interaction is similar for both the positron and electron, as the induced-multipole interaction is independent of the sign of the charge for closed shell atoms.

An important feature of our approach is that the effective cross sections are calculated in an *ab initio* manner from an interaction potential. This is useful because, (a) less is known about the positron elastic and annihilation cross sections, as measurements are more difficult than corresponding electron systems, and (b) it is the interaction between the charged particle and the atom that is modified in the fluid, whereas the isolated-atom cross sections are not so simply related to the effective cross sections in the fluid.

The structure of this article is as follows. We first describe the methods that allow us to obtain cross sections in the gas and dense fluid phases from scattering calculations and then how we can use these to obtain the transport coefficients in the gas and dense fluid phases. Comparison of calculated transport coefficient calculations under equilibrium and non-equilibrium conditions (driven out of equilibrium through the application of an applied field) with available experimental measurements represents a stringent test on the accuracy of our position cross-sections for dense gas and liquid phases. We validate our scattering calculations using gas phase data, for which both total cross section measurements and transport data are available [8, 9]. Then we apply the dense fluid formalisms, for which we can compare to experimental measurements in the dense gas [10] and liquid [11] regimes. The dense gas comparisons suggest, with reference to previous analysis [12], that there is an incompatibility with several of the measurements. We have been able to show that density effects are significant in the dense gas phase only at low reduced electric fields, by performing full calculations and through simple qualitative arguments. This has allowed us to suggest that an admixture of an impurity may resolve the discrepancies between our calculations and experimental measurements. We finally perform similar analysis for the liquid phase, and discuss the incompatibilities between the calculations and measurements.

2. Kinetic theory and transport properties

The kinetic equation used here to describe a positron swarm subject to an external electric field \mathbf{E} in a background of gaseous or liquid helium is Boltzmann's equation (BE) for the phase-space distribution function. As shown in our previous works [5, 6], comparison with positron swarm experiments can be made with only the steady-state, spatially-homogeneous solution:

$$\frac{q\mathbf{E}}{m} \cdot \frac{\partial f}{\partial \mathbf{v}} = -J(f), \quad (1)$$

where q and m are the charge and mass of the positron, by performing a Legendre polynomial P_l decomposition of the distribution function of positron velocities \mathbf{v} :

$$f(\mathbf{v}) = \sum_{l=0}^{\infty} f_l(\epsilon) P_l(\mu), \quad (2)$$

where $\epsilon = \frac{mv^2}{2}$, $\mu = \hat{\mathbf{v}} \cdot \hat{\mathbf{E}}$ and the collision integral $J(f)$ is given by the expansion

$$J(f) = \sum_{l=0}^{\infty} J^l(f_l). \quad (3)$$

Details of our calculation method can be found in [5, 6], which include a specialized collision operator for the coherent elastic scattering, denoted J^l in those articles, and relabelled as J_{el}^l in the current article. For the current investigation, we must also include the annihilation process for the positron, such that $J^l = J_{\text{el}}^l + J_{\text{an}}^l$. This requires the definition of the annihilation collision operator

$$J_{\text{an}}^l(f_l) = \nu_{\text{an}}(\epsilon) f_l, \quad (4)$$

where $\nu_{\text{an}}(\epsilon)$ is the energy-dependent annihilation collision frequency, which is related to an effective electron number, Z_{eff} , [13] via:

$$\nu_{\text{an}}(\epsilon) = Nv\sigma_{\text{an}}(\epsilon) = \pi r_0^2 c N Z_{\text{eff}}(\epsilon) \quad (5)$$

where N is the gas density, v is the relative speed, $\sigma_{\text{an}}(\epsilon)$ is the cross section for annihilation, $r_0 \approx 5.325a_0$ is the classical electron radius and c is the speed of light ($c = 1/\alpha$ in a.u. where α is the fine-structure constant).

The solution to BE allows a connection between microscopic scattering information, and macroscopic transport properties. The macroscopic transport quantity of interest in this work is the average annihilation rate α_{an} , which can be calculated from the energy distribution function, $f_0(\epsilon)$, via [3]

$$\alpha_{\text{an}} = 2\pi \left(\frac{2}{m}\right)^{\frac{3}{2}} \int_0^{\infty} \epsilon^{\frac{1}{2}} \nu_{\text{an}}(\epsilon) f_0(\epsilon) d\epsilon. \quad (6)$$

This quantity is more commonly described as an averaged effective electron number, $\langle Z_{\text{eff}} \rangle$, through the relation [13]

$$\alpha_{\text{an}} = \pi r_0^2 c N \langle Z_{\text{eff}} \rangle, \quad (7)$$

where these quantities depend on the distribution function and hence the electric field.

3. Scattering of positrons by individual helium atoms

The theoretical procedures used in this paper to describe the elastic scattering of positrons from helium atoms, at energies below the positronium formation threshold at 17.79 eV, are given in [14] and are essentially the same as those used in [5, 6] for electron scattering from argon and xenon. Thus, only a brief discussion of the overall method will be given here.

In the purely elastic energy region, only the static and polarisation potentials need to be included in the interaction for positron scattering. The scattering of the incident positrons, with wavenumber k , by helium atoms can then be described in the gaseous phase by the integral equation formulation of the partial wave Dirac–Fock scattering equations (see [14] for

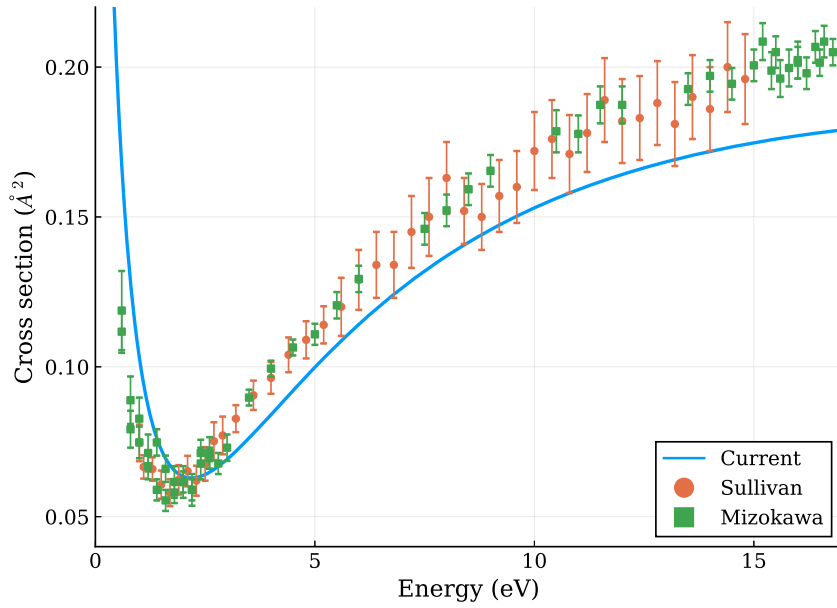


Figure 1. Comparison of our calculated gas phase cross sections [14] used in this paper to various experimental measurements [8, 9].

details). In matrix form, these equations can be written as

$$\begin{pmatrix} f_{\kappa}(r) \\ g_{\kappa}(r) \end{pmatrix} = \begin{pmatrix} v_1(kr) \\ v_2(kr) \end{pmatrix} + \frac{1}{k} \int_0^r dx G(r, x) \left[U(x) \begin{pmatrix} f_{\kappa}(x) \\ g_{\kappa}(x) \end{pmatrix} \right] \quad (8)$$

where $f_{\kappa}(r)$ and $g_{\kappa}(r)$ are the large and small components of the scattering wavefunction, $G(r, x)$ is the free particle Green's function and $U(r)$ is the local potential. In particular, $U(r)$ contains the static as well as the dipole and quadrupole polarisation interactions, with the latter being calculated by the polarized orbital method [15, 16]. The calculation of the momentum transfer cross section σ_{mt} from these potentials is discussed in [5, 6].

For positron scattering we also require the effective electron number,

$$Z_{\text{eff}} = \sum_{i=1}^N \int |\Psi(\mathbf{r}_1, \mathbf{r}_2, \dots, \mathbf{r}_N; \mathbf{x})| \delta(\mathbf{r}_i - \mathbf{x}) d\mathbf{r}_1 d\mathbf{r}_2 \dots d\mathbf{r}_N \quad (9)$$

Here Ψ is the total scattering wavefunction and the \mathbf{r}_i are the coordinates (including spin) of the atomic electrons while \mathbf{x} is the position vector of the incident positron. The quantity Z_{eff} can then be expressed as

$$Z_{\text{eff}} = Z_{\text{eff}}^0 + Z_{\text{eff}}^1 \quad (10)$$

where

$$Z_{\text{eff}}^i = \frac{1}{2\pi} \sum_{\kappa} \int_0^{\infty} dr \left[\frac{f_{\kappa}^2(r) + g_{\kappa}^2(r)}{r^2} \right] \rho_i(r). \quad (11)$$

Here $\rho_0(r)$ is the unperturbed charge density of the atomic orbitals and $\rho_1(r)$ is the first-order correction. In terms of the atomic wavefunctions $\rho_0(r)$ is given by

$$\rho_0(r) = \sum_{n\kappa} q_{n\kappa} [P_{n\kappa}^2(r) + Q_{n\kappa}^2(r)] \quad (12)$$

where $P_{n\kappa}(r)$ and $Q_{n\kappa}(r)$ are the large and small radial components of the atomic wavefunctions while $q_{n\kappa} = 2|\kappa|$ is the occupation number of the $n\kappa$ subshell of a closed shell atom.

The first-order charge density was determined by the non-relativistic polarized orbital method [15, 17], as relativistic effects are essentially negligible in light atomic systems. In the polarized-orbital method the first-order radial distortion $F_{nl}^{\nu\nu'}(r, x)$ of each atomic orbital $P_{nl}(r)$ is calculated adiabatically in the field of a point charge at a series of fixed points x (cf equation (12) of [15]). The corresponding non-relativistic scattering wavefunction $f_l(r)$ is normalized at infinity according to

$$f_l(r) \sim \frac{[4\pi(2l+1)]^{\frac{1}{2}}}{k} \sin \left[kx - \frac{l\pi}{2} + \delta_l \right]. \quad (13)$$

Here, k is the wavenumber of the incident positron while δ_l is the partial wave phase shift. The correction to the charge density is then found by keeping only terms to first order and is given by

$$\rho_1(r) = \sum_{nl} q_{nl} \sum_{\nu\nu'} (2\nu' + 1) \begin{pmatrix} \nu & \nu' & l \\ 0 & 0 & 0 \end{pmatrix}^2 P_{nl}(r) F_{nl}^{\nu\nu'}(r, r) \quad (14)$$

where $q_{nl} = 2(2l+1)$ is the occupation number of the nl subshell of a closed shell atom.

A comparison of the single-atom elastic cross sections to single-scatter experiments is shown in figure 1.

3.1. Transport coefficients

In order to test our calculation procedure in the dilute gas case, we can compare to various experimental measurements of the thermal zero-field annihilation rate [1, 18, 19] and to field-dependent measurements at 3.5 amagat of Davies *et al* [10]. The general consensus of the zero-field effective atomic number for room temperature is $\langle Z_{\text{eff}} \rangle_{T_0} \approx 3.9$ and our value

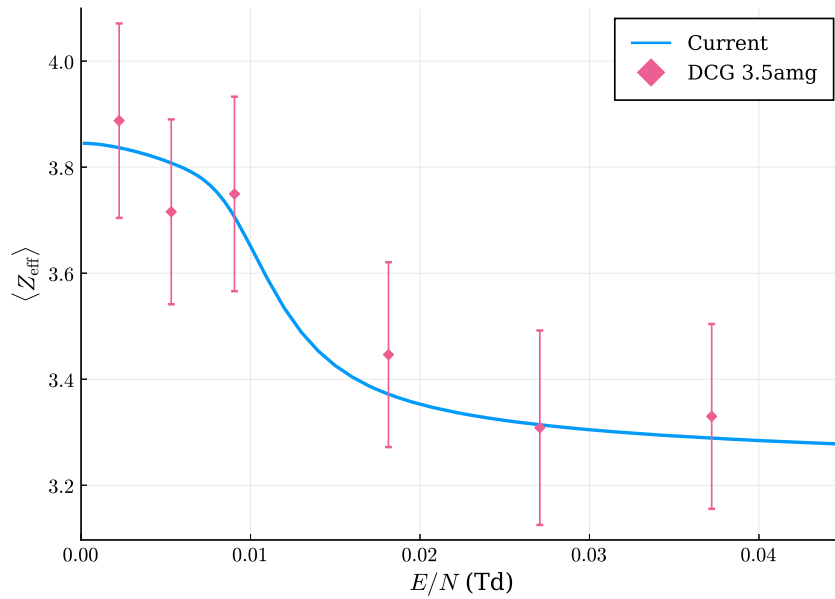


Figure 2. The averaged $\langle Z_{\text{eff}} \rangle(E)$ for gas phase compared to measurements [10]. The calculation is within the error bars of the measurements at 3.5 amg density.

of $\langle Z_{\text{eff}} \rangle_{T_0} = 3.84$ at 300 K is in good agreement. Our field-dependent results, shown in figure 2, are also in agreement with experiment, although the large uncertainties provide some leeway for variation.

We should note that the steady-state distribution, $f(v)$ in equation (2), is a non-equilibrium distribution, even in the non-equilibrium case owing to the ‘hole-burning’ effect provided by the energy-dependence of the annihilation collision frequency. Furthermore, it is also conceivable that the time-dependent behaviour of the positron swarm, as it approaches steady-state, could result in too few positrons that survive in order to reach the true steady-state $f(v)$ distribution. If this were the case, then the experimental measurements would correspond to an average over transient distributions instead of steady-state. Fortunately, it has been shown [12, 20] that enough positrons survive to accurately represent the steady-state distribution.

4. Scattering of positrons by dense helium fluids

Our approach to calculating the transport through liquids and dense gases, referred henceforth as dense fluids, is presented in [5, 6]. In these papers we detailed the procedure, originally proposed by [21] for constructing effective scattering potentials for electrons in dense media. The procedure is almost identical for positron scattering and we do not repeat the formalism here but describe only the changes we have made for the current application to positrons. These include (a) a contribution to the annihilation cross section from the average over surrounding atomic charge densities, (b) a different choice than our previous electron calculations for the outer radius of the scattering calculation, r_m , which represents the region of space ‘owned’ by the focus atom and distinguishes it from the rest of the bulk, and (c) a potential shift, ΔV , similar to that applied in our investigation of liquid krypton [7].

4.1. The averaged electron density ρ_{eff}

Analogous to the effective total potential, one can define an effective charge density with contributions from both the target atom and an ensemble average contribution from the atoms in the bulk, which acts to increase the positron annihilation rate in dense systems:

$$\begin{aligned} \rho_{\text{eff}}(R) &= \rho_L(R) + \rho_S(R) \\ &= \rho_L(R) + \frac{2\pi n}{R} \int_{r_m}^{\infty} ds \, sg(s) \int_{|R-s|}^{R+s} dt \, t \rho_L(t). \end{aligned} \quad (15)$$

Here $\rho_L = \rho_0 + \rho_1$ corresponds to the focus atom’s charge density and ρ_S denotes the surrounding average, shown as an integral in bipolar coordinates. The pair correlator, $g(s)$, indicates the probability to find another atom at a distance s from the focus atom. Note that the outer limit, r_m , of the scattering calculation effectively truncates $\rho_L(R)$ at $R = r_m$. This is complemented by the r_m lower limit on the outer integral of ρ_S , which indicates that only the charge density outside the region owned by the target atom contributes to the averaged density of its surrounding atoms. In other words, we consider any charge density within a range r_m of an atom to be ‘owned’ by that atom; this is necessary to prevent ‘double counting’ of the electrons for each atom. In the dilute gas limit $r_m \rightarrow \infty$ and $\rho_S \rightarrow 0$ as required.

With the total averaged charge distribution defined, we can easily extend the definition of Z_{eff} to include the total contribution from the focus and surrounding atoms:

$$\begin{aligned} Z_{\text{eff}} &= \frac{1}{n} \int_0^{r_m} dR \, (\rho_L(R) + \rho_S(R)) |\Psi(R)|^2 \\ &= Z_{\text{eff}}^L + Z_{\text{eff}}^S. \end{aligned} \quad (16)$$

We have found that in our current focus of helium, the contribution of Z_{eff}^S to the total Z_{eff} is negligible, however this may not be true for larger atoms.

We point out the analogy of the surrounding average to that performed for the potential itself, described in [5, 6]. To briefly summarise, the total potential $V(r) = U_1(r) + U_2(r)$ where $U_1(r)$ describes the screened interaction with the focus atom and $U_2(r)$ describes the potential after averaging over the surrounding atoms.

4.2. Choice of $r_m = r_{\text{WS}}$

In contrast to our previous works involving electrons in dense fluids, a different definition for r_m is required for positrons in dense fluids. In our previous works, we followed the lead of Lekner [4] to choose r_m as a turning point of the potential. However, in the current case of positron scattering, where the sign of the static potential is reversed, this definition results in a much larger value of r_m which appears to be physically invalid. Hence we make an alternative choice of setting r_m to the Wigner–Seitz radius, $r_{\text{WS}} = (4\pi N/3)^{-1/3}$. In the dense gas phase of helium at $N = 35.7$ amagat, this is $r_{\text{WS}} = 6.29$ Å and in the liquid phase at $N = 0.0188$ Å⁻³, this is $r_{\text{WS}} = 2.33$ Å. These radii, compared with the contributions to the potential of scattering in the liquid case, are shown in figure 3. We have also explored an alternative choice for the Wigner–Seitz radius [22], called the ‘local Wigner–Seitz radius’ $r_{\text{LWS}} = (4\pi N g_{\text{max}}/3)^{-1/3}$, where g_{max} is the maximum of the pair correlator $g(r)$. This quantity attempts to account for the increased density that the positron would feel in the majority of collisions. In our case, this results in a value of $r_{\text{LWS}} = 6.24$ Å in the dense gas phase, and $r_{\text{LWS}} = 2.08$ Å in the liquid phase.

We have explored the choice of r_{WS} before in our investigation of electrons in liquid argon, but found it to worsen the agreement between our calculations and experimental measurements. However, at that time we did not also apply an energy shift, which we discuss in the following section.

4.3. Potential shift

Even as the positron velocity approaches zero, it will feel a background energy in the presence of a liquid or dense gas [23]. This quantity is known as V_0 and has been obtained through a combination of measurement and calculation for electron scattering in various liquids, see [22, 24] and references therein. As it is not possible to do these same experiments with positrons, we instead investigate two different substitute values for V_0 and incorporate this into the scattering calculation as a potential shift, $\Delta V = V_0$. The first option for ΔV is $U_2(r \rightarrow 0)$, which corresponds to the averaged potential of the surrounding atoms felt at the origin, and the second surrogate is V_{WS} , a Wigner–Seitz calculation in the style of [22, 25], which we will describe in more detail in an upcoming paper. In short, the V_{WS} value is found as the minimum energy solution for a wavefunction that satisfies a ‘spherical Bloch wave’ boundary condition. We have applied a similar surrogate value for the potential shift, ΔV , when performing calculations of electrons in liquid krypton [7]. Note that the

value of V_{WS} itself depends on the value of r_m and we will refer to V_{WS} and V_{LWS} as the potential shift from using the regular (r_{WS}) and local (r_{LWS}) Wigner–Seitz radii respectively.

4.4. Pair correlators in helium

The essential input to perform the dense fluid calculations is the fluid pair-correlator and its Fourier transform, the static structure factor. For liquid-phase helium at $T = 4.2$ K, we use the pair-correlator and structure factor derived from experiments by [26]. For the dense gas case at $T = 295.65$ K, we have calculated the pair-correlator from Monte Carlo simulations with $N = 10000$ atoms using an untruncated Lennard–Jones potential with parameters [27] $\epsilon_{\text{LJ}}/k_{\text{B}} = 5.465$ K and $\sigma_{\text{LJ}} = 2.628$ Å. These pair correlators are shown in figure 4. As the pair correlator for the dense gas is relatively flat, it can be expected that some of the dense fluid effects will be negligible, however that contributions from the surrounding average will still be significant.

5. Results

5.1. Experimental measurements

There are several measurements of the zero-field annihilation rate, see [1, 28, 29] for a compilation, which allow us to assume a value of approximately $\langle Z_{\text{eff}} \rangle_{T_0} \approx 3.9$ for the dense gas phase and $\langle Z_{\text{eff}} \rangle_{T_0} \approx 3.6$ for the liquid phase. Our calculations, using several different choices for ΔV , span a range of different increases/decreases in the zero-field $\langle Z_{\text{eff}} \rangle_{T_0}$. In both phases, $\Delta V = 0$ shows an unusual increase in $\langle Z_{\text{eff}} \rangle_{T_0}$ which cannot be reconciled with the experimental measurements.

We are only aware of a few measurements of the non-equilibrium field-dependent annihilation rate. These are [10] for the dense gas phase and [11, 30] for the liquid phase. In both cases, there is a decrease in $\langle Z_{\text{eff}} \rangle(E)$ as the field is increased. While our calculations, shown in figures 5 and 6, also exhibit a decrease it happens (a) over a larger variation of $\langle Z_{\text{eff}} \rangle(E)$ for both dense gases and liquids and (b) with a shoulder at either too small or too large a field. In addition, the calculated variation of $\langle Z_{\text{eff}} \rangle(E)$ is much larger than experimentally observed. The similarity between the $\Delta V = V_{\text{WS}}$ and $\Delta V = V_{\text{LWS}}$ results in the dense gas was expected, as the key input distinguishing these approaches is the maximum in the pair correlator, which is negligible for the dense gas case. However, their behaviour in the liquid case is surprising: despite a 15% difference in r_m , the two cases share almost identical elastic and annihilation cross sections, leading to almost identical $\langle Z_{\text{eff}} \rangle$ values.

It is also possible for us to choose different values for our simulation parameters of r_m and ΔV , which are not necessarily physically motivated. We have done this by scanning a wide range of values but no particular choice allows us to obtain both the required magnitude and field-dependence of $\langle Z_{\text{eff}} \rangle(E)$, even approximately.

While the differences between our results and the experimental measurements in figures 5 and 6 appear to be quite

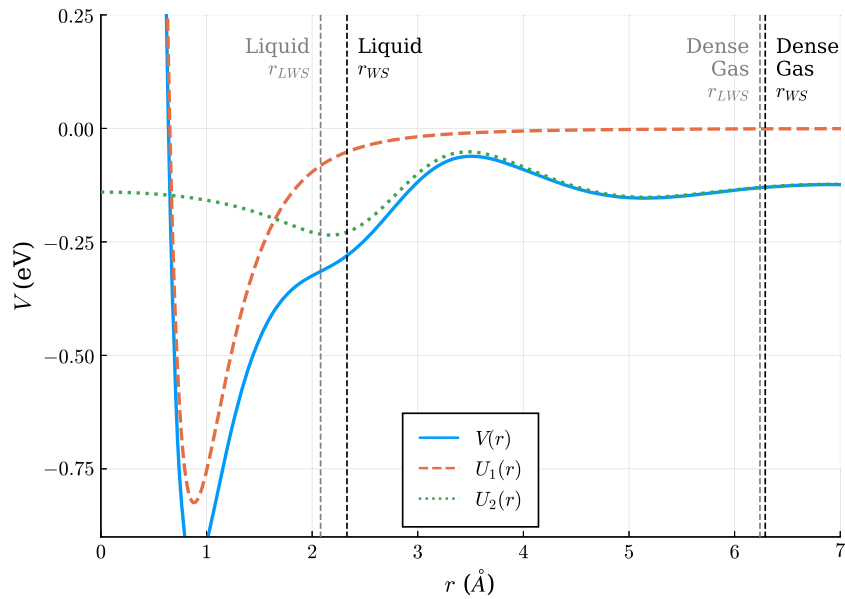


Figure 3. The potential due to the focus atom, $U_1(r)$, surrounding atoms, $U_2(r)$ and total scattering potential, $V(r)$ in the case of scattering in the liquid. The values of r_{WS} and r_{LWS} are shown as dashed vertical lines. For comparison the values of r_{WS} and r_{LWS} in the dense gas phase are also shown, however we point out that the surrounding and total potential curves are different in the dense gas phase.

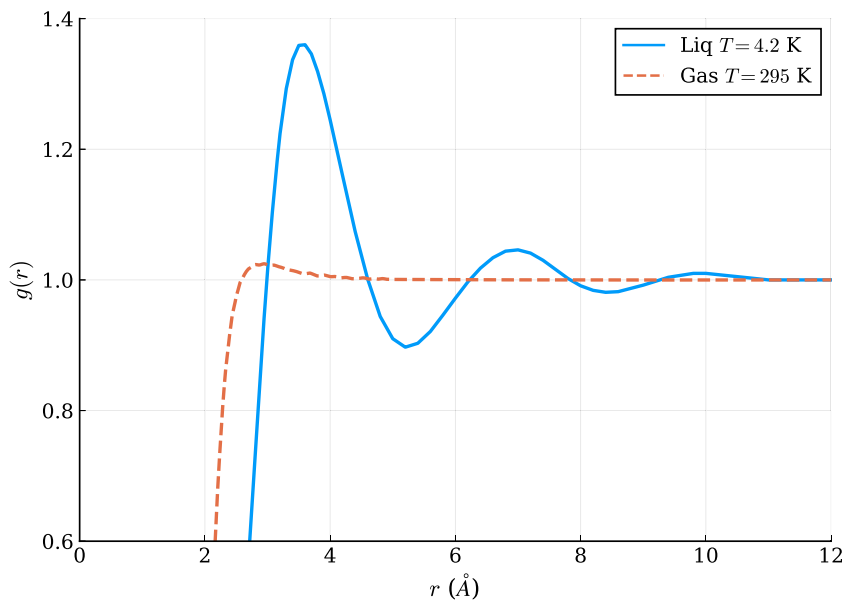


Figure 4. The pair correlators used for the liquid (solid blue line [26]) and dense gas (dashed orange line, calculated from Monte Carlo simulations) phases.

large, this is due to a relatively small variation in Z_{eff} . The differences between the $\Delta V = U_2(0)$ calculations and the measurements are within 5% for the dense gas case and 10% for the liquid case. This could be accounted for by assuming a systematic uncertainty in the measurements, but we will instead consider what modifications can be made to our model to reconcile experiment and theory in the following sections. It is worth pointing out that the analysis involved in these measurements may be complicated by the ordering of the lifetimes for free positron annihilation and o-Ps annihilation: in the low density 3.5 amagat case, o-Ps annihilation is faster, and in the

high-density 35.7 amagat case, free positron annihilation is faster [31].

We first discuss the dense gas case below in greater detail, and propose some modifications that we can make to explain the differences. We will then apply those considerations to the liquid phase.

5.2. Dense gas comparison

From figure 5, we can see that the various choices of ΔV allow us to tune the value of $\langle Z_{\text{eff}} \rangle(E)$ at low fields. However, these choices all result in the same behaviour of $\langle Z_{\text{eff}} \rangle(E)$ at high

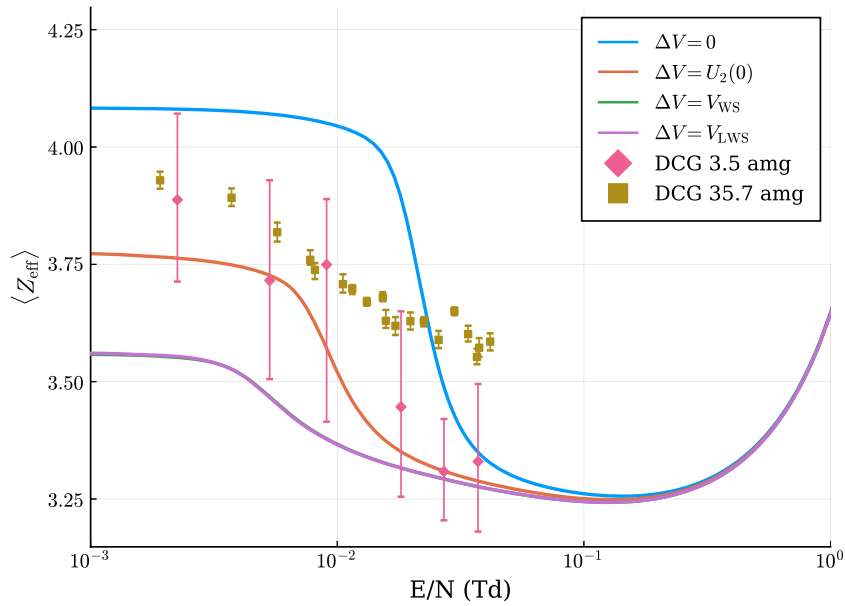


Figure 5. The comparison between dense gas measurements [10] and our calculations for various physically motivated choices of ΔV . These values should be compared directly with the 35.7 amg measurements but we also show the 3.5 amg measurements for reference. For the dense gas phase, $U_2(0) = -0.0084$ eV, $V_{\text{WS}} = -0.0151$ eV and $V_{\text{LWS}} = -0.0150$ eV. The similarity between the V_{WS} and V_{LWS} cases (they cannot be distinguished in the plot) is due to the insignificant peak in the pair correlator.

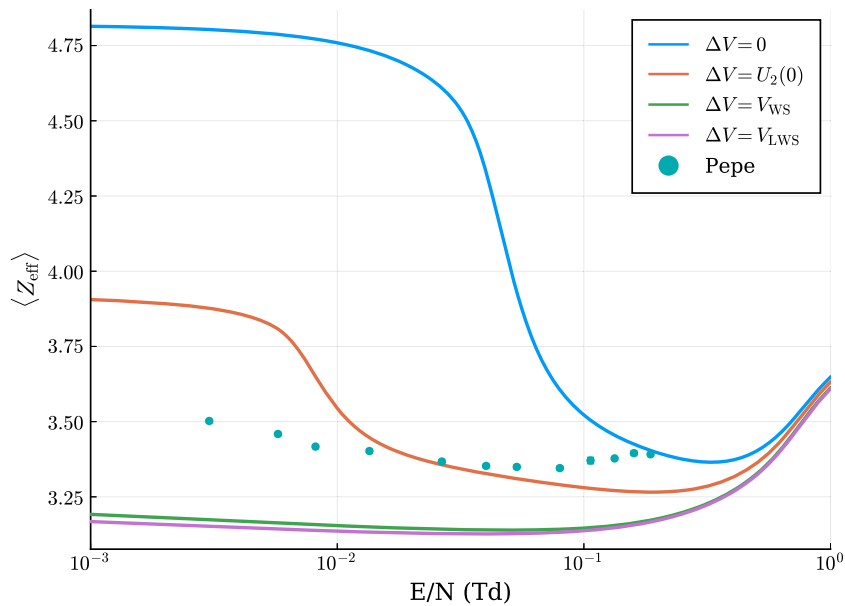


Figure 6. The comparison between liquid measurements [11] and our calculations for various physically motivated choices of ΔV . For the liquid phase, $U_2(0) = -0.14$ eV, $V_{\text{WS}} = -0.275$ eV and $V_{\text{LWS}} = -0.267$ eV.

fields. We believe this should be expected from modifications due to the dense fluid, as large kinetic energies overwhelm these effects. It is rather the difference in the experimental measurements at higher reduced fields between the 3.5 amagat and 35.7 amagat results that we find surprising.

We have explored some modifications to our model of the gas in order to obtain agreement with experiment. In terms of transport quantities, we require one or both of the following modifications: either (a) an additional source of annihilation which is significant at higher energies, or (b) a source of friction to reduce the mean energy at higher fields. A lower mean energy has the desired side effect of increasing the $\langle Z_{\text{eff}} \rangle$ felt

by the ensemble, as the annihilation cross section is larger at lower energies.

Both of these effects can be produced by a small admixture of an impurity in the gas. The dominant effects of a molecular species as an impurity can be represented by two additional processes: another annihilation pathway and an inelastic cross section. In order to separate these effects, we first consider the zero-field case. Here, the positron distribution (neglecting the small perturbation from annihilation) will remain close to a thermal distribution. In this way, the additional inelastic cross section can be neglected and only the additional annihilation pathway will affect the measured $\langle Z_{\text{eff}} \rangle_{T_0}$. This leaves us with

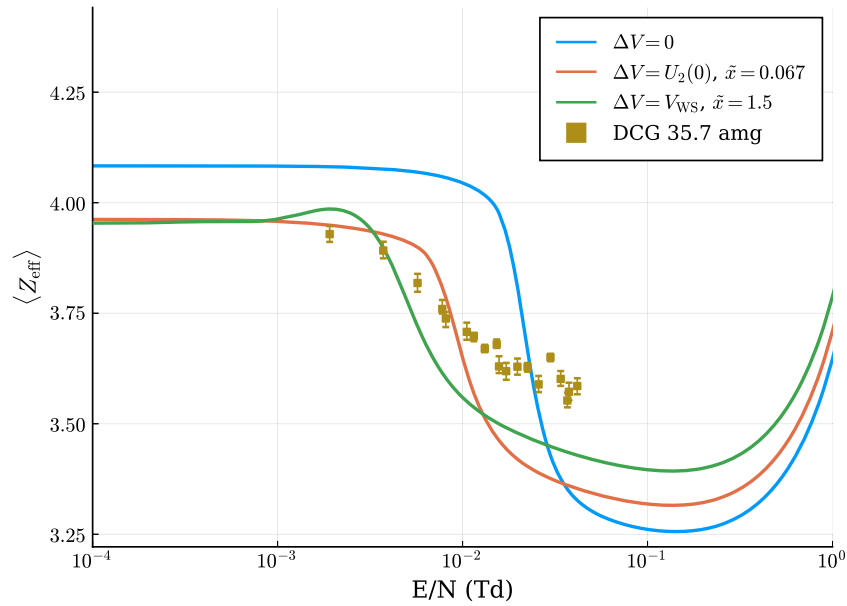


Figure 7. The effective electron number due to the small admixture of an impurity. The annihilation cross section is shaped like that of ethane and the effective ethane density is denoted as \tilde{x} in the legend. No additional inelastic processes are included in these results. Note that inclusion of an impurity can only increase the zero-field $\langle Z_{\text{eff}} \rangle$, so the $\Delta V = 0$ results cannot be made to match the zero-field experimental result.

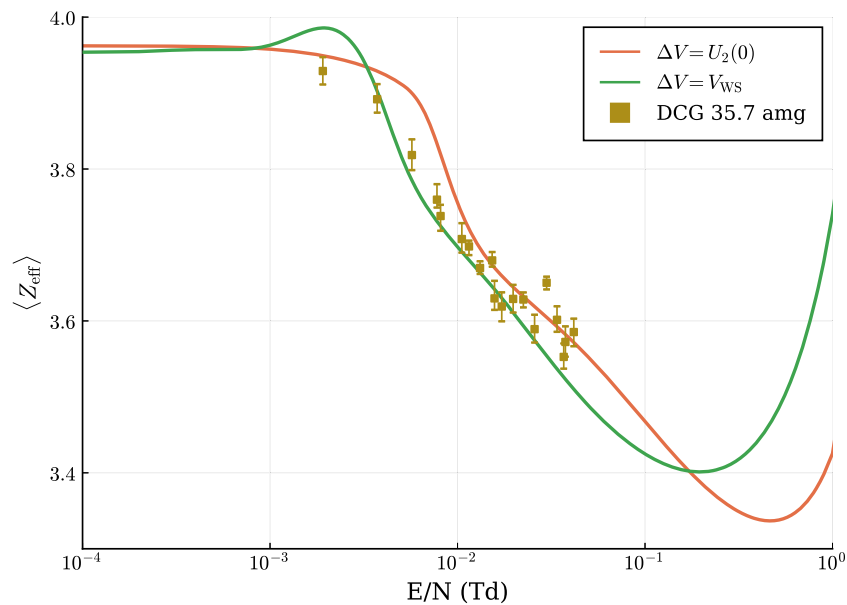


Figure 8. The effective electron number due to the small admixture of an impurity, including a constant inelastic cross section of magnitude \tilde{A} and threshold ϵ_{inel} . The $\Delta V = U_2(0)$ case corresponds to $\tilde{x} = 0.067\%$, $\tilde{A} = 10^{-3} \text{ \AA}^2$ and $\epsilon_{\text{inel}} = 2.5 \text{ eV}$ and the $\Delta V = V_{\text{WS}}$ case corresponds to $\tilde{x} = 0.15\%$, $\tilde{A} = 10^{-4} \text{ \AA}^2$ and $\epsilon_{\text{inel}} = 2 \text{ eV}$.

$$\langle Z_{\text{eff}} \rangle_{T_0} = \langle Z_{\text{eff}}^{\text{He}} \rangle_{T_0} + x \langle Z_{\text{eff}}^{\text{imp}} \rangle_{T_0} \quad (17)$$

where x is the ratio of impurity density to helium density.

As it is likely that a mix of different hydrocarbons can play the role of impurities, we substitute their combined $\langle Z_{\text{eff}}^{\text{imp}} \rangle$ by a cross section that is proportional to that of ethane, i.e. $Z_{\text{eff}}^{\text{imp}}(\epsilon) = CZ_{\text{eff}}^{\text{C}_2\text{H}_6}(\epsilon)$, and reinterpret $\tilde{x} = xC$ as an **effective** ethane impurity density. While this introduces an ambiguity into the impurity, it removes one fitting parameter from our calculations. We emphasize that even a few fitting parameters can allow us to fit any measured $\langle Z_{\text{eff}} \rangle(E)$, so it is important to limit the number of these as much as possible.

Our simulations, after fitting for \tilde{x} at $E = 0$, are shown in figure 7. We can see that only a very small admixture is required to match the experimental value of $\langle Z_{\text{eff}} \rangle_{T_0}$. However, in the case of $\Delta V = 0$, no amount of impurity will lower the $\langle Z_{\text{eff}} \rangle_{T_0}$ value.

We now turn to including the second-most significant aspect of an impurity, which is the introduction of inelastic collisions with lower threshold energies than helium. As we again want to consider a range of hydrocarbon impurities, we use a surrogate cross section of constant magnitude \tilde{A} and threshold ϵ_{inel} . We again reinterpret this quantity as the magnitude $\tilde{A} = xA$ which is an **effective** inelastic cross section, indicating a magnitude

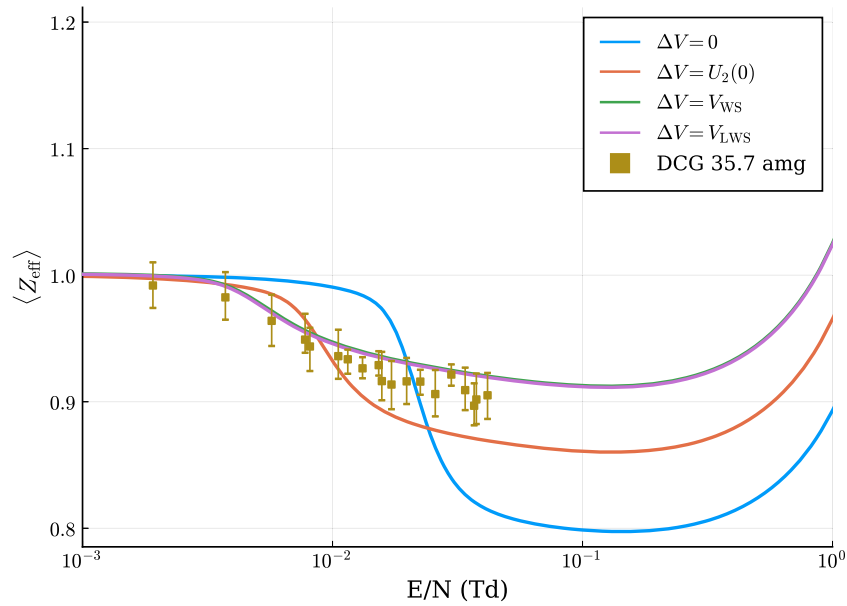


Figure 9. The effective electron number as shown in figure 5 but scaled to the zero-field value $\langle Z_{\text{eff}} \rangle_{T_0}$. No impurity is included in these calculations. This is useful in the scenario that the comparison between absolute values is not possible. In this scenario, the $\Delta V = V_{\text{WS}}$ and $\Delta V = V_{\text{LWS}}$ cases represent the best fit.

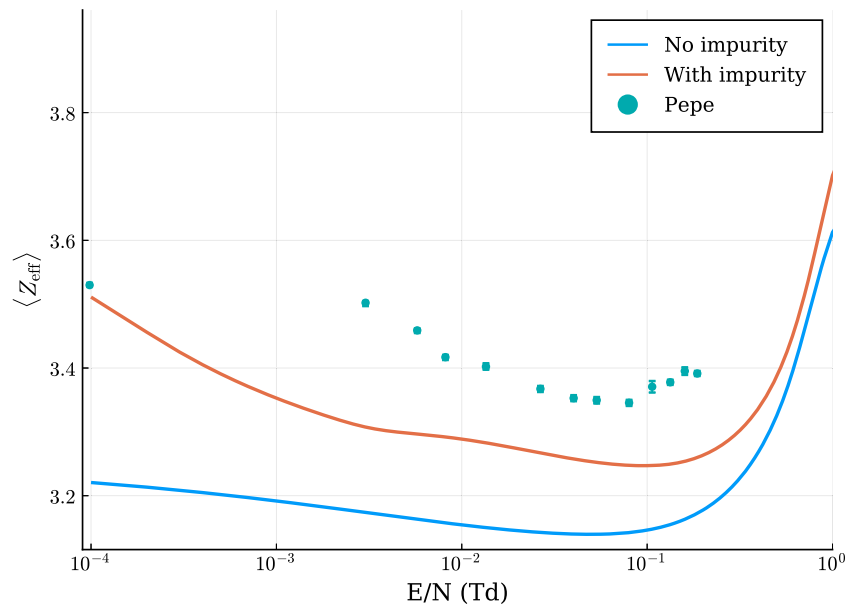


Figure 10. The effective electron number in liquid helium, due to the small admixture of an impurity and using $\Delta V = V_{\text{WS}}$. The impurity parameters are $\tilde{x} = 0.1\%$, $\tilde{A} = 10^{-4} \text{ \AA}^2$ and $\epsilon_{\text{inel}} = 2 \text{ eV}$. Although the inclusion of the impurity can adjust the zero-field rate to bring it into agreement with the experimental measurement, the rest of the field range is not in agreement, even with the inclusion of an inelastic process. The uptick in the experimental measurements at the higher fields has been shown to be due to Ps formation as the positrons reached a steady-state distribution.

relative to the density of helium. By doing this, there are only three parameters to characterise the impurity: \tilde{x} , \tilde{A} and ϵ_{inel} . The value of \tilde{x} is fixed by the zero-field annihilation rate, so we now vary the latter two parameters to obtain the best fits shown in figure 8.

In all cases, the fits perform reasonably well and provide good agreement over most of the range of experimental measurements. The fit for $\Delta V = V_{\text{WS}}$ includes an additional peak at around $E/N = 2 \times 10^{-3} \text{ Td}$ not seen in the experimental

data, while the $\Delta V = U_2(0)$ curve does not follow the data as closely.

As an alternative, we can choose to believe that the comparison of absolute values from our calculation and measurement may not be well posed, and instead we can compare the $\langle Z_{\text{eff}} \rangle(E)$ values relative to the zero-field $\langle Z_{\text{eff}} \rangle_{T_0}$. This is shown in figure 9, where the $\Delta V = V_{\text{WS}}$ and $\Delta V = V_{\text{LWS}}$ appear to give the closest fit, although all choices are not unreasonable.

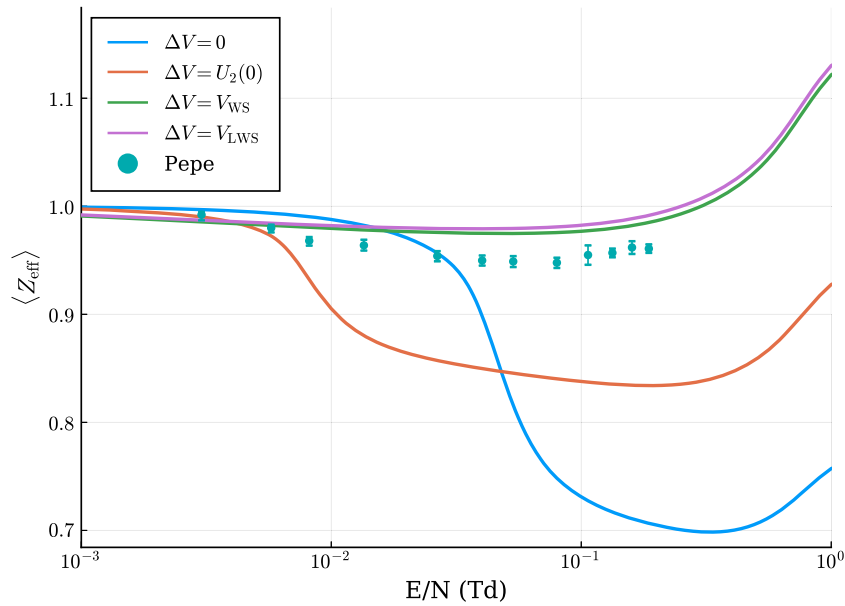


Figure 11. The effective electron number as shown in figure 5 but scaled to the zero-field value $\langle Z_{\text{eff}} \rangle(E = 0)$. No impurity is included in these calculations.

5.3. Liquid comparison

As with the dense gas case, we can apply the same steps to include an impurity to better match the experimental measurements. There is less likelihood for the presence of an impurity in liquid helium, as it would be expected to freeze out of the liquid. In any case, we can consider the effect it would have.

For the liquid the $\Delta V = U_2(0)$ case produces a zero-field value which is higher than the experiment, even without the inclusion of an impurity. This means that we can only consider the $\Delta V = V_{\text{WS}}$ case as suitable to add an impurity.

The effect of the impurity in the $\Delta V = V_{\text{WS}}$ case is shown in figure 10, with and without the additional of an inelastic process. It is clear to see that we cannot obtain agreement. This is somewhat surprising, as we have some free parameters to manipulate. We believe this suggests that there is a contribution missing from our calculations, which is due to multiple scattering at high densities.

We should also point out that we should not aim to fit the uptick in the experimental results at high fields. This has been shown [11] to be an apparent increase only, and is actually due to the formation of positronium with ionised electrons. This spur-enhanced Ps formation is estimated to be at most 1% and only occurs at higher fields. As the apparent $\langle Z_{\text{eff}} \rangle$ is about 1.2% larger at the higher fields, this fits almost perfectly with this explanation.

We can also consider the possibility of positrons forming self-trapped clusters of higher density in the helium liquid [32]. However, these clusters have been found to only be present for densities less than that of liquid helium. Hence, we can ignore this mechanism as a source of increased Z_{eff} .

Finally, we note that we have not accounted for a difference between the applied and effective electric fields due to the permittivity of the liquid. This is because the effect is negligible, as the dielectric constant [33] of helium is $1.05 \approx 1$.

Again, we have made a comparison with the relative difference to the zero-field $\langle Z_{\text{eff}} \rangle$ value, shown in figure 11. In contrast to the similar comparison in figure 9, there is a much bigger difference in the choices of ΔV for calculation, but the $\Delta V = V_{\text{WS}}$ and $\Delta V = V_{\text{LWS}}$ choices remain closest to the experimental measurements.

While the inability to fit the liquid results is problematic for our calculation method, we still believe that our approach to obtain agreement for the dense gas case is valid. This is because the density of 35.7 amg in the measurements of [10] is a rather dilute density, so multiple-scattering effects should also be relatively weak. However, we cannot completely rule out the possibility that our dense gas calculations are also lacking some additional physical behaviour.

6. Conclusions

We have modelled the transport of positrons under an applied electric field through dense fluids of helium and compared our predictions of annihilation rates to experimental measurements in the dense gas and liquid phases. Our model includes modifications due to coherent scattering and screening of the interaction potential between the positron and the helium atom, which have been discussed in previous articles. This article has introduced additional considerations for the annihilation rate due to electrons from the surrounding atoms, and we have shown that double counting should be avoided in the averaging process.

While our model does not provide results in complete agreement with experimental measurements, we are able to include a very small ($\approx 0.1\%$) contribution of an impurity that is representative of a hydrocarbon to vastly improve this agreement. The impurity is motivated by the noticeable difference between the dilute gas and dense gas measurements and is represented using a model which includes three fitting parameters.

Our model has been extended from our previous articles, to include one adjustable parameter, ΔV , for which we have explored three physically-motivated values: (a) $\Delta V = U_2(0)$, (b) $\Delta V = V_{WS}$ and (c) $\Delta V = V_{LWS}$. These values are (a) the total polarisation potential of the surrounding atoms at the origin of the focus atom and (b) the ground state energy of the conduction band, calculated in a Wigner–Seitz model and (c) a calculation in the Wigner–Seitz model using a ‘local’ Wigner–Seitz radius [22]. In both the dense gas and the liquid, the effects of $\Delta V = V_{WS}$ and $\Delta V = V_{LWS}$ were found to be nearly identical. In the case of a dense gas of helium, any of these choices can be made to agree with the experimental measurements, using different choices of an impurity admixture. However, for the case of liquid helium, only the choices of $\Delta V = V_{WS}$ or $\Delta V = V_{LWS}$ were found to be compatible, yet there remained significant discrepancies between our calculated values and the experimental measurements.

Our results, using the Boltzmann equation description outlined in this article, have also been independently verified using a Monte-Carlo calculation. Details of that implementation are available in [34, 35].

One of the reasons that impurities can play a large role in our current investigations is due to the very small Z_{eff} of helium. In the future, we wish to model positron transport through fluids of larger atomic species. These atoms, with many more electrons, may provide a means to better test our calculations by suppressing the potential effects of impurities.

In addition, we wish to explore further choices of ΔV and determine a method to uniquely specify its value. One manner in which to do this is to consider species in which there are a larger range of densities with experimental measurements, such as krypton [36]. We also intend to include further multiple-scattering corrections to both ΔV and Z_{eff} [37, 38], to see if these can identify the current disagreement between our calculations and experimental measurements.

Acknowledgments

We would like to acknowledge valuable discussions with Prof. M Charlton regarding the possibility of impurities in the dense gas experimental measurements. DGC and RDW acknowledge funding from the Australian Research Council through its Discover Project (DE170101024 and DP190100696) schemes.

ORCID iDs

D G Cocks  <https://orcid.org/0000-0002-9943-7100>

G J Boyle  <https://orcid.org/0000-0002-8581-4307>

R D White  <https://orcid.org/0000-0001-5353-7440>

References

- [1] Charlton M and Humberston J W 2001 *Positron Physics* (Cambridge: Cambridge University Press)
- [2] Prantzos N *et al* 2011 The 511 keV emission from positron annihilation in the Galaxy *Rev. Mod. Phys.* **83** 1001
- [3] Robson R, White R and Hildebrandt M 2017 *Fundamentals of Charged Particle Transport in Gases and Condensed Matter* (Boca Raton, FL: CRC Press)
- [4] Lekner J 1967 Motion of electrons in liquid argon *Phys. Rev.* **158** 130
- [5] Boyle G J, McEachran R P, Cocks D G and White R D 2015 Electron scattering and transport in liquid argon *J. Chem. Phys.* **142** 154507
- [6] Boyle G J, McEachran R P, Cocks D G, Brunger M J, Buckman S J, Dujko S and White R D 2016 *Ab initio* electron scattering cross-sections and transport in liquid xenon *J. Phys. D: Appl. Phys.* **49** 355201
- [7] White R D *et al* 2018 Electron transport in biomolecular gaseous and liquid systems: theory, experiment and self-consistent cross-sections *Plasma Sources Sci. Technol.* **27** 053001
- [8] Mizogawa T, Nakayama Y, Kawaratani T and Tosaki M 1985 Precise measurements of positron–helium total cross sections from 0.6 to 22 eV *Phys. Rev. A* **31** 2171
- [9] Sullivan J P, Makochekanwa C, Jones A, Caradonna P and Buckman S J 2008 High-resolution, low-energy positron scattering from helium: measurements of the total scattering cross section *J. Phys. B: At. Mol. Opt. Phys.* **41** 081001
- [10] Davies S A, Charlton M and Griffith T C 1989 Free positron annihilation in gases under the influence of a static electric field *J. Phys. B: At. Mol. Opt. Phys.* **22** 327
- [11] Pepe I, Paul D A L, Steyaert J, Gimeno-Nogues F, Deutsch J and Prieels R 1995 Positron annihilation in liquid helium and liquid argon under an electric field *J. Phys. B: At. Mol. Opt. Phys.* **28** 3643–59
- [12] Boyle G J, Casey M J E, White R D and Mitroy J 2014 Transport theory for low-energy positron thermalization and annihilation in helium *Phys. Rev. A* **89** 022712
- [13] Charlton M 1999 Experimental studies of positrons scattering in gases *Rep. Prog. Phys.* **48** 737
- [14] McEachran R P and Stauffer A D 2019 Positron scattering from helium *J. Phys. B: At. Mol. Opt. Phys.* **52** 115203
- [15] McEachran R P, Ryman A G, Stauffer A D and Morgan D L 1977 Positron scattering from noble gases *J. Phys. B: At. Mol. Phys.* **10** 663
- [16] McEachran R P, Morgan D L, Ryman A G and Stauffer A D 1978 *J. Phys. B: At. Mol. Phys.* **11** 951
- [17] McEachran R P, Ryman A G and Stauffer A D 1978 Positron scattering from neon *J. Phys. B: At. Mol. Phys.* **11** 551
- [18] Paul D A L and Graham R L 1957 Annihilation of positrons in liquid helium *Phys. Rev.* **106** 16
- [19] Charlton M 2009 Positron transport in gases *J. Phys.: Conf. Ser.* **162** 012003
- [20] Green D G 2017 Positron cooling and annihilation in noble gases *Phys. Rev. Lett.* **119** 2
- [21] Cohen M H and Lekner J 1967 Theory of hot electrons in gases, liquids, and solids *Phys. Rev.* **158** 305
- [22] Evans C M and Findley G L 2010 Energy of the conduction band in near critical point fluids *Phys. Res. Int.* **2010** 1–6
- [23] Iakubov I T and Khrapak A G 1982 Self-trapped states of positrons and positronium in dense gases in liquids *Rep. Prog. Phys.* **45** 697
- [24] Borghesani A F 2006 Electron and ion transport in dense rare gases *IEEE Trans. Dielectr. Electr. Insul.* **13** 492
- [25] Plenkiewicz B, Frongillo Y, Lopez-Castillo J M and Jay-Gerin J P 1996 A simple but accurate ‘core-tail’ pseudopotential approach to the calculation of the conduction-band energy V_0 of quasifree excess electrons and positrons in nonpolar fluids *J. Chem. Phys.* **104** 9053
- [26] Sears V F, Svensson E C, Woods A D B and Martel P 1979 The static structure factor and pair correlation function for liquid ^4He at saturated vapour pressure *Technical Report November* Atomic Energy of Canada Ltd

- [27] Oh S-K 2013 Modified Lennard–Jones potentials with a reduced temperature-correction parameter for calculating thermodynamic and transport properties: noble gases and their mixtures (He, Ne, Ar, Kr, and Xe) *J. Thermodyn.* **2013** 1
- [28] Fox R A, Canter K F and Fishbein M 1977 Positron and orthopositronium decay rates in helium at high densities *Phys. Rev. A* **15** 1340
- [29] Nieminen R M 1980 Nonlinear density dependence of the positron decay rate in helium *Phys. Rev. A* **21** 1347
- [30] Pepe I, Paul D A L, Gimeno-Nogues F, Deutsch J and Prieels R 1994 Positron annihilation in helium, argon and nitrogen liquids under an electric field *Hyperfine Interact.* **89** 425
- [31] Charlton M 2020 private communication
- [32] Manninen M and Hautojärvi P 1978 Clustering of atoms around the positron and positive ions in gaseous He, Ne, and Ar *Phys. Rev. B* **17** 2129
- [33] Chase C E, Maxwell E and Millett W E 1961 The dielectric constant of liquid helium *Physica* **27** 1129
- [34] Tattersall W J, Cocks D G, Boyle G J, Brunger M J, Buckman S J, García G, Petrović Z L, Sullivan J P and White R D 2017 Spatial profiles of positrons injected at low energies into water: influence of cross section models *Plasma Sources Sci. Technol.* **26** 045010
- [35] Tattersall W J, Cocks D G, Boyle G J, Buckman S J and White R D 2015 Monte Carlo study of coherent scattering effects of low-energy charged particle transport in Percus–Yevick liquids *Phys. Rev. E* **91** 043304
- [36] Jacobsen F M, Gee N and Freeman G R 1986 Electron mobility in liquid krypton as function of density, temperature, and electric field strength *Phys. Rev. A* **34** 2329
- [37] Ziman J M 1966 Wave propagation through an assembly of spheres I. The Greenian method of the theory of metals *Proc. Phys. Soc.* **88** 387
- [38] Lax M 1951 Multiple scattering of waves *Rev. Mod. Phys.* **23** 287